α-planar states in ^{28}Si

G. S. Anagnostatos*
Department of Physics, University of Oxford, Nuclear Physics Laboratory, Keble Road, Oxford, OX1 3RH, United Kingdom

P. Ginis and J. Giapitzakis
University of Patras, School of Engineering, Patra, 26110, Greece
(Received 17 July 1997; revised manuscript received 1 June 1998)

α-planar states in ^{28}Si are studied by employing the isomorphic shell model which uses no adjustable parameters. In the model, possible α particles and their spatial distribution are derived, instead of being assumed as usual in α-cluster models. Oblate triaxial structure for the ground state and a seven α-particle planar structure for states with hexadecapole deformation have been found. Predictions of ground state and excited rotational bands and of other observables have been made and results are successfully compared with experimental data and those of other models where available. The novelty of the present study is focused on the fact that the axis of rotation changes within the ground state band and that the mentioned α-planar structure originates four rotational bands two of which exhibit an almost rigid body rotation supporting a superdeformation for ^{28}Si. The resonances of $^{12}C+^{16}O$ at 32.20 MeV, $I^{\pi}=16^{+}$, and at 46.2 MeV and 43.6 MeV, $I^{\pi}=14^{+}$, decaying to known planar states of light $4n$ nuclei, have been verified as members of three of the above four excited bands, thus supporting the proposed planar structure of ^{28}Si. [S0556-2813(98)02312-7]

PACS number(s): 21.60.Gx, 21.10.Re, 27.30.+t

I. INTRODUCTION

The existence of superdeformed configurations in light nuclei is of great current interest. Such configurations have particularly been studied in $A=4n$-nuclei and have mostly been associated with highly deformed α-cluster structures, specifically with α-chain and α-planar states in these nuclei. The α-cluster models have a long history in nuclear physics [1–16], however, for a review of the α-chain nuclei one could refer to Ref. [17], while for a review of the α-planar nuclei to Ref. [18]. Most of these studies have been performed by using the Bloch-Brink α-cluster model [9]. However, all previous studies are rather model dependent and only that of Ref. [19] (based on reduced widths for α decay of ^{20}Ne to the ground state of ^{16}O) constitutes the most thorough and instructive one concerning the structure of α-cluster nuclei and stands as a basic reference for any objective study of all $A=4n$ (where $n=1-10$) nuclei. In very recent publications [20,21] an alternative approach along the lines of the isomorphic shell model has been applied in studying α-chain states in ^{12}C and α-planar states in ^{20}Ne. In the present work the same approach is applied in studying α-planar states in ^{28}Si, which is one of the most interesting and most studied nuclei in the *sd*-shell region [22].

The common point between the isomorphic shell model and the α-cluster model is that both models consider the geometry of the average positions of the constituent particles as the starting point for describing the total wave function of the nucleus. The basic difference between these two models is that the constituent particles for the first are nucleons in shell model orbitals [23], while the constituent particles for the second model are α-particles usually taken in *s*-state. Of course, even in the Bloch-Brink model the α-particles may be thought of as dissolving into nucleons since, for cluster separations reaching zero, the antisymmetrization forces the cluster wave function into some shell model limit.

The geometries in the α-cluster models arise through the long-range effects of antisymmetrization and the mean field, combined with a preference for simple underlying structures [24]. In these models several geometries are chosen for the α-particles involved in a particular nucleus and the final selection is made with reference to the maximum binding energy. In the isomorphic shell model, instead, a common geometry for all nuclei is derived by packing the nuclear shells, whose average forms result from the independent particle assumption [25]. The specific part of this geometry utilized by the average positions of the nucleons constituting a particular nucleus results from the search for the maximum binding energy and other observables [20–21]. α-like particles thus appear by themselves each time the average positions of two protons and of two neutrons (possessing the same principal quantum number *n* and, in addition, all four nucleons involved have the same angular momentum which implies that each pair of nucleons have zero relative angular momentum, i.e., each pair of nucleons is in relative *s*-state) are found close together. Of course, for later moments than that depicted by the nucleon average positions each nucleon of an α-like particle follows an independent particle motion in a well-defined shell-model orbital leading to dissolution of this α-particle.

In the present stage of development of the α-cluster models predictions on α-planar states in $4n$ nuclei are limited to the density distribution of such nuclei, to the specification of some experimental levels which are candidates for rotational spectra, and to their related ground state binding energies [18]. In the present work, by employing the isomorphic shell

*Permanent address: Institute of Nuclear Physics, National Center for Scientific Research Demokritos, Aghia Paraskevi, Attiki, 15310 Greece. FAX:++(301)6511215. Electronic address: anagnos@cyclades.nrcps.ariadne-t.gr

model, binding energies, radii, electric moments, mean lifetimes, $B(E2)$ values, and rotational spectra are studied for the nucleus ^{28}Si. That is, here more observables are examined and, in addition as will become apparent, our predictions for the observables investigated by other models are much closer to the experimental data. Moreover, new rotational bands are introduced, and known resonances in nuclear reactions at specific spins and energies are verified as members of these bands offering additional support for planar structures of specific states in ^{28}Si.

II. THE ISOMORPHIC SHELL MODEL

The isomorphic shell model is a microscopic nuclear-structure model that incorporates into a hybrid model the prominent features of single-particle and collective approaches in conjunction with the nucleon finite size [23,25]. The model consists of a quantum mechanical part [23] and a semiclassical part [25] and the relationship between these two parts is obtained in the spirit of the Ehrenfest's theorem.

The model has been reported in several previous publications (see, for example, cited references of the model in the review article [26]). The very recent ones [20,21] contain, perhaps, the most concise representation of the model. Thus, here it seems sufficient to include only the main features of the model together with the technical part (formulas) of its semiclassical part (that includes also features of the model), which is here applied for ^{28}Si since this part is closer to the α-cluster model and thus a comparison between them is easier and more comprehensive. Of course, the isomorphic shell model is not limited to applications to $4n$-nuclei but it is a general model for all nuclei [23,25,27–30].

A. Main features of the model

The single-particle component of the model is along the lines of the conventional shell model with the only difference that in the model the nucleons creating the central potential are the nucleons of each particular nuclear shell alone, instead of all nucleons in the nucleus as assumed in the conventional shell model [23]. In other words, we consider (for the case where a harmonic oscillator is taken as the central potential) a multiharmonic potential description of the nucleus (as many potentials as shells), as follows:

$$H\Psi = E\Psi, \quad H = T + V, \tag{1}$$

$$H = H_{1s} + H_{1p} + H_{1d2s} + \cdots, \tag{2}$$

where

$$H_i = V_i + T_i = -\overline{V} + \frac{1}{2}\,\mathbf{m}(\omega_i)^2 r_i^2 + T_i\,. \tag{3}$$

That is, we consider a state-dependent Hamiltonian, where each partial harmonic oscillator potential has its own state-dependent frequency ω_i. All these ω_i's are determined from the harmonic oscillator relation [31]

$$\hbar\omega_i = \frac{\hbar^2}{\mathbf{m}\langle r_i^2\rangle}\left(n_i + \frac{3}{2}\right), \tag{4}$$

where n_i is the harmonic oscillator quantum number and $\langle r_i^2\rangle^{1/2}$ is the average radius of the relevant high fluximal shell determined by the semiclassical part of the model specified below. For details on $\overline{V}$ one should consult Ref. [23].

The solution of the Schrödinger equation with Hamiltonian (3), in spherical coordinates, for each partial single particle Hamiltonian H_i is

$$\Psi_{n_i l_i m_i}(r_i, \theta_i, \phi_i) = R_{n_i l_i}(r_i) Y_{l_i}^{m_i}(\theta_i, \phi_i), \tag{5}$$

where the coordinates r_i, θ_i, ϕ_i refer to a single particle, $Y_{l_i}^{m_i}(\theta, \phi)$ are the familiar spherical harmonics, and the expressions for the $R_{n_i l_i}(r)$ are given in several books of quantum mechanics and nuclear physics; for example, see Tables 4-1 of Ref. [31].

The only difference between our wave functions and those in these books is the different ω_i's as stated in Eqs. (3) and (4) above. Those of our wave functions, however, which have equal l value, because of the different $\hbar\omega_i$, are not orthogonal, since in these cases the orthogonality of Legendre polynomials does not suffice. Orthogonality, of course, can be obtained by applying established procedures, e.g., the Gram-Schmidt process [32].

By employing the partial Hamiltonian shown in Eqs. (2) and (3) all eigenvalues involved in a specific nucleus can be calculated. Finally, the binding energy of this nucleus can be estimated by using the simple relationship

$$E_B = 1/2(\overline{V}\cdot N) - 3/4\left[\sum_{i=1}^{A} \hbar\omega_i (n + 3/2)\right], \tag{6}$$

where $\overline{V}$ is the average potential depth. That is, the binding energy is not taken equal to the sum of single-particle energies [33]. This is suggested by variation of the energy in the framework of the Hartree-Fock method. Specifically, Eq. (6) is in the lines of Koopman's theorem [31] which helps us to understand the origin of the coefficients 1/2 and 3/4.

In the framework of the quantum mechanical part of the isomorphic shell model [23], by using the harmonic oscillator wave functions with different ω_i, we can exactly determine the matrix elements in a completely microscopic way. Thus, we can obtain the expectation values of different observables without any approximation. This is already done in previous publications [23,27–30]. Here, however, the semiclassical part (i.e., an approximate model) instead of the quantum mechanical part (i.e., an exact model) is employed since the former involves a pictorial approach which is similar to the α-cluster model, a fact which facilitates the comparison of their results. This use of the semiclassical part in the place of the quantum mechanical part is accepted in the spirit of the Ehrenfest's theorem [20,21,34,35]. This theorem for the special case of a harmonic oscillator potential, as here employed in Eq. (3), is particularly well described in Ref. [35]. From the discussion made there for such a potential, one could extract that (in a semiclassical treatment) the nuclear structure problem could be reduced into that of studying the dynamics of the average positions of the con-

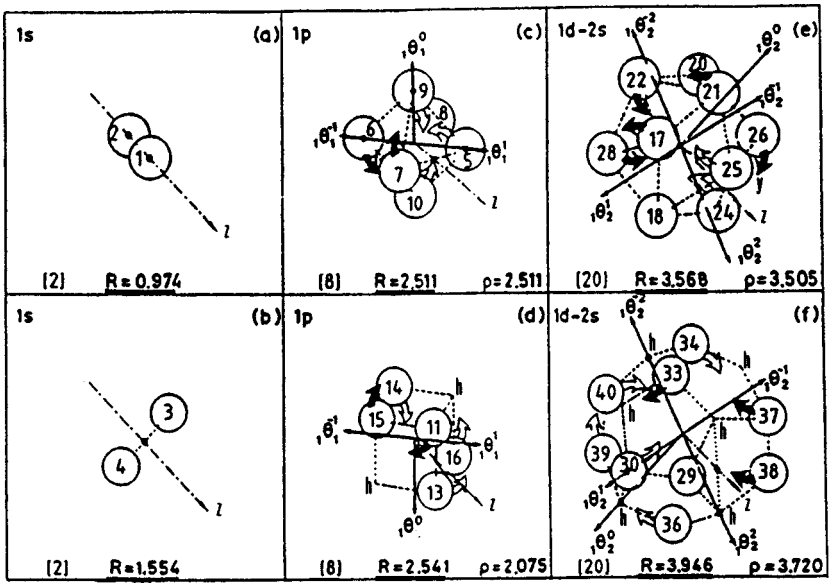

FIG. 1. The isomorphic shell model for the nuclei up to $N=20$ and $Z=20$. The high-symmetry polyhedra in row 1 (i.e., the zerohedron, the octahedron, and the icosahedron) stand for the average forms of (a) the $1s$, (c) the $1p$, and (e) the $1d2s$ shells for neutrons, while the high-symmetry polyhedra in row 2 [i.e., the zerohedron, the hexahedron (cube), and the dodecahedron] stand for the average forms of (b) the $1s$, (d) the $1p$, and (f) the $1s2s$ shells for protons. The vertices of polyhedra stand for the average positions of nucleons in definite quantum states (τ,n,l,m,s). The letters *h* stand for the empty vertices (holes). The *z* axis is common for all polyhedra when these are superimposed with a common center and with relative orientations as shown. At the bottom of each block the radius *R* of the sphere circumscribed to the relevant polyhedron and the radius ρ of the relevant classical orbit [equal to the maximum distance of the vertex state $(r,n,l.m,s)$ from the axis ${}_n\theta_l^m$ precisely representing the orbital angular-momentum axis with definite *n*, *l*, and *m* values] are given. The curved arrows shown help the reader visualize around which axis each nucleon rotates, while solid (open) arrows show rotations directed up (down) the plane of the paper. All polyhedra vertices are numbered as shown. The backside (hidden) vertices of the polyhedra and the related numbers are not shown in the figure.

stituent nucleus. For this study the following two assumptions are employed by the semiclassical part of the isomorphic shell model.

(i) The neutrons (protons) of a closed neutron (proton) shell, considered at their *average* positions, are in *dynamic equilibrium* on the sphere presenting the average size of that shell.

(ii) The average sizes of the shells are determined by the *close-packing* of the shells themselves, provided that a neutron and a proton are represented by *hard spheres* of definite sizes (i.e., $r_n=0.974$ fm and $r_p=0.860$ fm).

It is apparent that assumption (i) is along the lines of the conventional shell model, while assumption (ii) is along the lines of the liquid-drop model.

The model employs a specific equilibrium of nucleons, considered at their average positions on concentric spherical cells, which is valid whatever the law of nuclear force may be: assumption (i). This equilibrium leads uniquely to Leech [25,36] (equilibrium) polyhedra as average forms of nuclear shells. All such nested polyhedra are closed-packed, thus taking their minimum size: assumption (ii). The cumulative number of vertices of these polyhedra, counted successively from the innermost to the outermost, reproduce the magic numbers each time a polyhedral shell is completed [25] (see the numbers in the brackets in Fig. 1 there).

For one to conceptualize the isomorphic shell model, he should first relate this model to the conventional shell model. Specifically, the main assumption of the simple shell model, i.e., that each nucleon in a nucleus moves (in an average potential due to all nucleons) independently of the motion of the other nucleons, may be understood here in terms of a *dynamic equilibrium* in the following sense [25]. Each nucleon in a nucleus is *on average* in a *dynamic equilibrium* with the other nucleons, and, as a consequence, its notion may be described independently of the motions of the other nucleons. From this one realizes that dynamic equilibrium and independent particle motion are consistent concepts in the framework of the isomorphic shell model.

In other words, the model implies that *at some instant in time* (reached *periodically*) all nucleons could be thought of as residing at their individual average positions, which coincide with the vertices of an equilibrium polyhedron for each shell. This system of particles evolves in time according to each particle independent motion. This is possible, since axes standing for the angular-momenta quantization of directions are *identically* described by the rotational symmetries of the polyhedra employed [36–39]. For example, see Ref. [38], where one can find a complete interpretation of the independent particle model in relation to the symmetries of these polyhedra. Such vectors are shown in Fig. 1 for the orbital angular-momentum quantization of directions involved for nuclei up to $N=20$ and $Z=20$.

Since the radial and angular parts of the polyhedral shells in Fig. 1 are well defined, the coordinates of the polyhedral vertices (nucleon average positions) can be easily computed. These coordinates up to $N=Z=20$ are already published in footnote 14 of Ref. [40], and in Refs. [41] and [42]. These coordinates correspond to the *R* values of the exscribed polyhedral spheres given in Fig. 1 (see bottom line at each block).

According to the semiclassical part of the isomorphic shell model, the nucleon average positions of a nucleus are distributed at the vertices of the polyhedral shells as shown, for example, in Fig. 1. The specific vertices occupied, for a given (closed- or open-shell) nucleus at the ground state, form a vertex configuration (corresponding to a state configuration) that possesses the maximum binding energy (E_B) in relation to any other possible vertex configuration, which thus stands for an excited state. Each vertex configuration defines the average form and structure of a relevant state of this nucleus. All bulk (static) properties of this state (e.g., E_B, rms radii, etc.) are derived as properties of this structure, as has been fully explained in Ref. [25] and references cited therein.

B. Technical features of the semiclassical part of the model

The model employs a two-body potential in the form of two Yukawa functions [40]:

$$V_{ij}=1.7(10^{17})\,\frac{e^{-(31.8538)r_{ij}}}{r_{ij}}-187\,\frac{e^{-(1.3538)r_{ij}}}{r_{ij}}\quad(\text{in MeV}), \tag{7}$$

where the average internucleon distances r_{ij} are estimated by using the relevant coordinates.

The Coulomb potential between two proton average positions apparently is

$$(E_C)_{ij}=\frac{e^2}{r_{ij}}, \tag{8}$$

where r_{ij} stand for the average interproton distances estimated by using the relevant coordinates.

The average kinetic energy for each nucleon is taken as the sum of the kinetic energy due to the uncertainty principle and of the kinetic energy due to the orbiting of the nucleon [42]:

$$\langle T\rangle_{nlm}=\frac{\hbar^2}{2m}\left[\frac{1}{R_{\max}^2}+\frac{l(l+1)}{\rho_{nlm}^2}\right], \tag{9}$$

where $R_{\max}$ is the outermost polyhedral radius (R) plus the relevant average nucleon radius (i.e., $r_n=0.974$ fm or $r_p=0.860$ fm), i.e., the radius of the nuclear volume in which the nucleons are confined, m is the nucleon mass, ρ_{nlm} is the distance of the vertex (n,l,m) from the axis ${}_n\vartheta_l^m$ (see Fig. 1 and Refs. [36–39], [42]).

The spin-orbit interaction in the model is given below [31]:

$$(E_{\mathrm{SO}})_i=(20\pm5)A^{2/3}\vec{l}_i X\vec{s}_i\,. \tag{10}$$

The energy coefficient ($20\pm5=15-25$ MeV) starts at its lower values for the lower orbital angular momenta and tends more or less smoothly to the larger values for the higher orbital angular momenta. As also known, for $j=l+1/2$, $l\cdot s=+l/2$, while for $j=l-1/2$, $l\cdot s=-(l+1)/2$.

The collective rotational energy is given by Eq. (11):

$$E_{\mathrm{rot}}=\frac{\hbar^2 I(I+1)}{2\mathcal{I}}, \tag{11}$$

where $\mathcal{I}$ is the moment of inertia of the rotating part of the nucleus given by Eq. (12):

$$\mathcal{I}=\sum_i^{N_{\mathrm{rot}}}\mathbf{m}r_i^2=\mathbf{m}N_{\mathrm{rot}}\langle r^2\rangle_{\mathrm{rot}}, \tag{12}$$

where N_{rot} is the number of nucleons participating in the collective rotation and $\langle r^2\rangle_{\mathrm{rot}}$ is the rms radius of these nucleons. This value of $\mathcal{I}$ is increased by the quantity (0.165) N_{rot}, where the coefficient 0.165 stands for the contribution to the moment of inertia coming from the finite size of each nucleon participating in the rotation [20,21].

The binding energy in the model, now, is

$$E_B=-\sum_{\substack{\text{all nucleon}\\ \text{pairs}}}V_{ij}-\sum_{\substack{\text{all proton}\\ \text{pairs}}}\frac{e^2}{r_{ij}}-\sum_{\text{all nucleons}}\langle T\rangle_{nlm}+\sum_{\substack{\text{all valence}\\ \text{pairs}}}E_{(\mathrm{SO})_i}, \tag{13}$$

where the terms E_δ (odd-even) and E_{rot} (collective rotation) appearing in Eq. (15) of Ref. [20] for the binding energy are here omitted as irrelevant to the case of interest, i.e., ^{28}Si.

The rms charge radius is given by Eq. (14):

$$\langle r^2\rangle_{\mathrm{ch}}^{1/2}=\left[\frac{\Sigma_{i=1}^{Z}R_i^2}{Z}+(0.8)^2-(0.116)\,\frac{N}{Z}\right]^{1/2}, \tag{14}$$

where R_i is the radius of the ith proton average position from Fig. 1, Z and N are the proton and the neutron numbers of the nucleus, and $(0.8)^2$ and (0.116) are the rms charge radii of a proton and of a neutron, respectively [43].

The intrinsic electric quadrupole moment is given by Eq. (15):

$$eQ'_{20}=\sum_i eQ'_{(20)i}=\sum_{i=1}^{Z}eR_i^2(3\cos^2\theta_i-1), \tag{15}$$

where R_i is the radius of the ith proton average position and θ_i is the corresponding azimuthal angle with respect to the symmetry axis [44].

The intrinsic electric hexadecapole moment is given by Eq. (16):

$$eQ'_{40}=\sum_i eQ'_{(40)i}=\sum_{i=1}^{Z}eR_i^4(35\cos^4\theta_i-30\cos^2\theta_i+3), \tag{16}$$

where R_i and θ_i as for Q'_{20} above.

The reduced electric-quadrupole transition probability between the 0^+-ground state and the first 2^+-state in even-even nuclei which exhibit a rotational [44] spectrum is given by Eq. (17):

$$\begin{aligned}B(E2)_{\mathrm{ex}}(\mathrm{cm}^4)&=4.08\times10^{-61}[E_\gamma(\mathrm{MeV})]^{-5}[\tau(\mathrm{sec})]^{-1}[1+a_T]^{-1}\\&=Q_0'^2 5/(16\pi)=\beta_2^2[3ZR_0^2/4\pi]^2,\end{aligned} \tag{17}$$

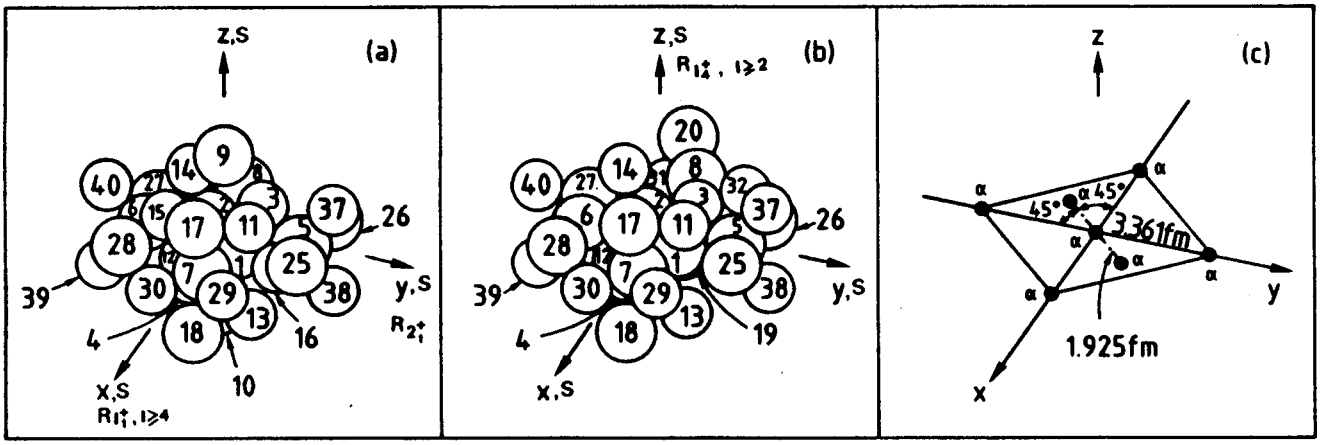

FIG. 2. Average forms of ^{28}Si, according to the semiclassical part of the isomorphic shell model, composed of the average positions of the constituent nucleons. (a) stands for the ground state and (b) for the 0_4^+ excited state at 10.27 MeV [called in the next Fig. 2(b)-relaxed] or for the proposed 0^+ state at 24.2 MeV [called in the text Fig. 2(b)]. Average nucleon positions are numbered as shown by using the same number as in Fig. 1 for the same position, except for the average positions named 3_r and 4_r in (b)-relaxed (see text for their coordinates), where these positions are ''relaxed,'' i.e., they are in contact with those numbered 5, 8 and 6, 7, respectively. Otherwise, parts (a) and (b) differ only in that positions 9-10, 15-16 appear only in (a) and positions 19-20, 31-32 appear only in (b). (c) comes from (b) or (b)-relaxed when each of the seven sets of four close-by nucleons (two neutrons and two protons) in relative *s*-state numbered (5,7,11,13), (6,8,12,14), (17-18, 29-30), (19-20, 31-32), (25-26, 37-38), (27-28, 39-40), and (1-2, 3-4) for (b) or (1-2, 3_r-4_r) for (b)-relaxed are assumed to form a sort of an α-particle. Axes labeled *x*, *y*, *z* stand for the axes of coordinates and $C2$ symmetry axes, while those labeled $R_{2_1^+}$, $R_{I_1^+,I\geq 4}$, and $R_{I_4^+,I\geq 2}$ for rotational axes.

where E_γ and τ are the excitation energy and the mean life of the first 2^+-state, a_T is the internal conversion coefficient, and β_2 is the deformation parameter which for a spheroid nucleus with semimajor and semiminor axes a and b takes the expression [44]

$$\beta_2 = 1.06(a-b)/R_0, \tag{18}$$

where $R_0 = r_0 A^{1/3}$ is the nuclear average radius.

Equations (7)–(17) stand for all formulas here necessary for the implementation of the semiclassical part of the model.

III. CALCULATIONS AND DISCUSSION

The average structure of ^{28}Si, in the framework of the semiclassical part of the isomorphic shell model, comes from Fig. 1 by considering the states ($1s$, $1p$, and $1d$) involved in this nucleus. From all possibilities offered by Fig. 1 to accommodate 14 neutron average positions on the neutron polyhedra [see Figs. 1(a), 1(c), and 1(e)] and 14 proton average positions on the proton polyhedra [see Figs. 1(b), 1(d), and 1(f)], the one shown in Fig. 2(a), as has been calculated, possesses the maximum binding energy and thus stands for the ground state of ^{28}Si.

Figure 2(b) comes also from Fig. 1 and differs from Fig. 2(a) only in four nucleon average positions, that is, instead of the positions numbered 9-10 and 15-16 utilized in Fig. 2(a), the positions numbered 19-20 and 31-32 are employed in Fig. 2(b). This leads to a ^{12}C core in Fig. 2(b) for ^{28}Si, instead of ^{16}O core in Fig. 2(a). That is, in Fig. 2(b) the states $2s_{1/2}$ appear instead of the states $1p_{1/2}$ appearing in Fig. 2(a). This difference in the core, as will be understood shortly, makes Fig. 2(a) three-dimensional and Fig. 2(b) two-dimensional in an α-cluster-wise representation.

Specifically, in Fig. 2(b) each set of the following four nucleon average positions numbered (1-4), (5,7,11,13), (6,8,12,14), (17-18,29-30), (19-20,31-32), (25-26,37-38), (27-28,39-40) accommodates two protons and two neutrons which are close together for the instant depicted by this figure and possess the same *n* and *j* quantum numbers. That is, each pair of these nucleons have zero relative angular momentum, i.e., it is in a relative *s*-state. Thus, in the model each of these seven sets of four nucleons can be considered as a sort of α-particle [20,21]. Considering now the center of gravity for each of these ''α-particles,'' Fig. 2(c) results, where the centers of the above seven α-like particles *precisely* lie on the same plane (i.e., these centers are coplanar). Of course, for later moments than that depicted by Fig. 2(b), each of the four nucleons composing any one of the above seven α-particle-like structures evolves by following its independent particle motion in a well-specified shell model orbital [36–39]. That is, each nucleon will move in a shell model orbital rotating around its own axis of orbital angular momentum vector as schematically shown by arrows in Fig. 1 and labeled by the proper ${}_n\theta_l^m$ angle with respect to the quantization axis *z* common for all parts of Fig. 1.

It is worth noticing that Fig. 2(c) is geometrically well specified. It consists of a square (with four α-like particles at its corners) with the length of its half diagonal equal to 3.361 fm and an interior straight segment (of half length equal to 1.925 fm) bisecting the right angle formed by the crossing of the two diagonals of the square (with two α-like particles at the ends of the segment and one at its center). This straight segment *precisely* stands for the α-particle representation of ^{12}C according to the semiclassical part of the isomorphic shell model [20,21].

It is interesting for one to compare the present Fig. 2(c) with Fig. 1 of Ref. [18], where an α-cluster study of ^{28}Si is also performed. The relevant part of that figure is reproduced here as Fig. 3 to make the comparison easier for the reader.

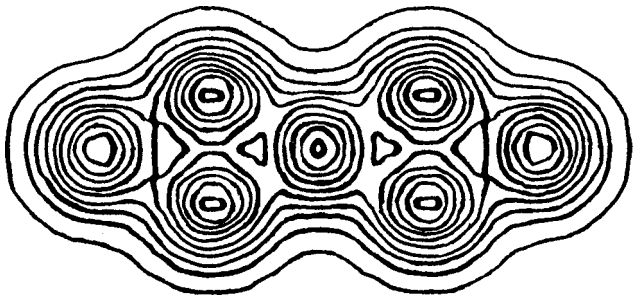

FIG. 3. Cluster density contours for the two-dimensional configuration (c) in Fig. 1 of Ref. [18] for ^{28}Si.

Both figures [Fig. 2(c) and Fig. 3] include an orthogonal parallelogram of four α-like particles and a bisecting straight segment of three α-like particles. However, in Fig. 3 the straight segment extends outside the parallelogram, while in Fig. 2(c) it is surrounded by the parallelogram. The sizes of the parallelograms and of the line segments are also different in these two figures.

As in the study of ^{12}C in Figs. 2(a) and 2(b) of Ref. [20], from the present Fig. 2(b) another figure can result which is almost identical to it and only slightly differs with respect to the average positions of the two $1s$ protons (numbered 3 and 4). Specifically, due to the absence of $1p_{1/2}$ neutrons from the ^{12}C core of Fig. 2(b) (numbered 9 and 10 in Fig. 1) whose average positions together with those of $1p_{3/2}$ neutrons (numbered 5-8) determine the symmetry of the average positions for the $1s$ protons, these two latter positions can relax (by rotation around their center of gravity on the plane which is perpendicular on the direction 1-2 and passes through the nuclear center) by getting closer to the average positions for the $1p_{3/2}$ neutrons (numbered 5,8 and 6,7, respectively) in such a way that their corresponding nucleon bags come in contact. The corresponding new coordinates of 3 and 4 are $3r$: $x=-1.006$ fm, $y=1.006$ fm, $z=0.3737$ fm and 4_r: $x=1.006$ fm, $y=-1.006$ fm, $z=-0.3737$ fm, where the subscript r stands for the word relaxed. This relaxation of the two proton average positions leads to larger binding energy for ^{28}Si. Since the corresponding figure could not be distinguished from Fig. 2(b), it is omitted and we let Fig. 2(b) stand for both cases, but in the text the distinction is made as Fig. 2(b) and Fig. 2(b)-relaxed. This increase of binding energy effectively comes from an increase of the potential energy alone, the only quantity which significantly varies from Fig. 2(b) to Fig. 2(b)-relaxed. Coulomb energy, Q'_{20}, and Q'_{40} do not have a noticeable variation. It is interesting for one to remark that both Fig. 2(b) and Fig. 2(b)-relaxed identically contain the same sort of α-particles and thus both figures identically lead to Fig. 2(c).

By applying Eqs. (7)–(10) one obtains the numerical values for each of the four first terms in Eq. (13), and for each of the three vertex (and state) configurations of column 1 (and 2), which are listed in columns 3-6 of Table I. The summation of the above four terms gives the net energy which for each configuration of column 1 is listed in column 7 of the same table. From the values of this column, it is apparent that the second and third configurations of Table I, which come from the two-dimensional (2D; α-cluster-wise) Fig. 2(b)-relaxed and Fig. 2(b), respectively, correspond to excited states, while the first configuration, which comes from the three-dimensional (3D) Fig. 2(a), corresponds to the ground state. The latter is so due to the fact that (as already mentioned) this configuration has the maximum net energy for any other possible 3D configuration for ^{28}Si involving $1s$, $1p$, and $1d$ states and coming from Figs. 1(a)–1(f). It should also be noticed that Fig. 2(b) and Fig. 2(b)-relaxed are the only 2D configurations (α-particle-wise) which can be obtained for ^{28}Si. The excitation energy (with respect to the ground state) of the second configuration, i.e., $E_{\rm ex}=10.4$ MeV, is almost identical to that of the 0^+_4, i.e., $E_{\rm ex}=10.27$ MeV, while the model ground-state energy, i.e., 245.2 MeV, is 8.66 MeV larger than the experimental one,

TABLE I. Vertex configuration, state configuration, potential (PE), Coulomb (CE), kinetic (KE), spin orbit (SOE), and net (NE) energy, geometrical sketch, and α-cluster-wise dimensionality for three configurations of ^{28}Si.

Vertex configuration	State configuration	PE (MeV)	CE (MeV)	KE (MeV)	SOE (MeV)	NE (MeV)	Geom. sketch	α-cluster dimensionality
(Core: 1-16) (17-18,29-30),(25-26,37-38), (27-28,39-40)	$(1s)^2_{n,p}(1p)^6_{n,p}(1d_{5/2})^6_{n,p}$	492.2	33.9	237.1	24.0	245.2	α-^{16}O-α	3D
exp.[a]						236.54[a]		
[Core:(1-2,3$_r$-4$_r$),(5,7,11,13), (6,8,12,14)], (17-18,29-30), (19-20,31-32),(25-26,37-38), (27-28,39-40)	$(1s)^2_{n,p}(1p)^4_{n,p}(1d_{5/2})^6_{n,p}(2s)^2_{n,p}$	479.0	31.7	242.9	30.4	234.8	α-^{12}C$_{(r)}$-α	2D
exp.[a]						226.27[b]		
[Core:(1-2,3-4),(5,7,11,13), (6,8,12,14)], (17-18,29-30) (19-20,31-32), (25-26,37-38), (27-28,39-40)	$(1s)^2_{n,p}(1p)^4_{n,p}(1d_{5/2})^6_{n,p}(2s)^2_{n,p}$	465.2	31.7	242.9	30.4	221.0	α-^{12}C-α	2D

[a]See Ref. [64].
[b]See Ref. [45].

TABLE II. Root mean square charge radius ($\langle r^2\rangle_{\rm ch}^{1/2}$), intrinsic electric quadrupole moment (Q'_{20}), intrinsic electric hexadecapole moment (Q'_{40}), reduced electric-quadrupole transition probability [$B(E2)$], mean lifetime (τ), and deformation parameter (β_2) for three configurations of ^{28}Si.

Vertex configuration	$\langle r^2\rangle_{\rm ch}^{1/2}$ (fm)	Q'_{20} (fm^2)	Q'_{40} (fm^4)	$B(E2)$ (fm^4)	τ (ps)	β_2
(Core: 1-16), (17-18,29-30),(25-26,37-38),(27-28,39-40)	3.21	-69.6	395.5	482	0.77	-0.49
exp.	3.15(5)[a]	-63 ± 18[b]		395 ± 226[b]	0.58 ± 0.33[b]	$-.45\pm0.11$[b]
[Core:(1-2,3$_r$-4$_r$)(5,7,11,13),(6,8,12,14)], (17-18,29-30)(19-20,31-32), (25-26,37-38),(27-28,39-40)	3.41	-104.8	2152.6	1093		0.74
exp.					<0.06 ps[c]	
[Core:(1-2,3-4),(5,7,11,13),(6,8,12,14)], (17-18,29-30),(19-20,31-32), (25-26,37-38),(27-28,39-40)	3.41	-100.8	2109.7	1011		0.72

[a]See Ref. [43].
[b]See Refs. [60,65].
[c]See Ref. [45].

i.e., 236.54 MeV. The third configuration of Table I leads to even higher excitation, i.e., 24.2 MeV, where there are not any experimental data for comparison.

As seen from Figs. 2(a) and 2(b), the existence of deformation of the average shapes for the ground state [Fig. 2(a)] and for the excited states [Fig. 2(b) and Fig. 2(b)-relaxed] of ^{28}Si is apparent. However, there is a difference between these two deformations. Specifically, α-particle-wise, Fig. 2(a) possesses a triaxial oblate deformation, while Fig. 2(b) and Fig. 2(b)-relaxed possess a plane structure which, of course, also has an oblate deformation [see Fig. 2(c) and Q'_{20} sign and values in Table II]. In Figs. 2(a) and 2(b) the axes of symmetry and the corresponding axes of rotation are also shown. Specifically, in Fig. 2(a) the axis of coordinates y is shown as axis of symmetry as well since the nucleon average positions numbered 17-18, 29-30 shown in the figure have an equivalent effect on all observables as the positions numbered 19-20, 31-32 not shown in this figure. Thus, the corresponding 4 nucleons (2 protons and 2 neutrons) could be thought of as 50% occupying the average positions 17-18, 29-30 and 50% occupying the positions 19-20, 31-32, hence the origin of the symmetry axis y and the oblate shape of Fig. 2(a). The same reasoning holds true for the axis of symmetry labeled z in Fig. 2(a). For the axis of symmetry labeled x in Fig. 2(a) or the axes of symmetry labeled x,y,z in Fig. 2(b) and Fig. 2(b)-relaxed, the situation is more transparent. Precisely speaking, the symmetry axes x,y,z in both Figs. 2(a) and 2(b) are $C2$ axes concerning the nucleon average positions of the $2s1d$ shell and simultaneously $C4$ axes concerning the nucleon average positions of the $1p$ shell. This is due to the fact that the $1s$ nucleons can have either the average positions shown numbered 1-2, 3-4 (or 3$_r$-4$_r$) in Figs. 1(a) and 1(b), and in Figs. 2(a), 2(b), and 2(b)-relaxed or their symmetric counterparts with respect to the axis x or y or z.

As apparent from Fig. 2(a), the axis of rotation labeled $R_{2_1^+}$ is perpendicular to the axes of symmetry labeled x and z, but simultaneously is an axis of symmetry itself (labeled y). Also, the axis of rotation labeled $R_{I_1^+,I\geq 4}$ is perpendicular to the axes of symmetry labeled y and z, but simultaneously is an axis of symmetry itself (labeled x). Similarly, the axis of rotation labeled $R_{I_4^+,I\geq 2}$ in Fig. 2(b) is perpendicular to the axes of symmetry x and y, but simultaneously is an axis of symmetry itself (labeled z). Thus, a clarification is needed to explain why here an axis of symmetry can be an axis of rotation as well.

As already mentioned, the reported axes of rotation R are $C2$ axes of symmetry of the whole average form of ^{28}Si as presented either in Figs. 2(a) or 2(b) [that is, each of these rotational axes is a $C2$ symmetry axis simultaneously for the average forms of all ($1s$, $1p$, and $2s1d$) nuclear shells]. This means that none of these axes has the C_∞ symmetry appearing, e.g., in an axially symmetric ellipsoidal. Thus, rotation around each of these $C2$ symmetry axes is quantum mechanically permissible [20,21] and each such rotation could lead to an observable.

By applying Eqs. (14)–(17) and (11) and (12) the quantities $\langle r^2\rangle_{\rm ch}^{1/2}$, Q'_{20}, Q'_{40}, $B(E2)$, τ, β_2, $\mathcal{I}$, and E_{I^+} (for $I=0-16$) are computed and listed in Table II, columns 2–7 and in Table III, columns 2–12, for each of the configurations presented by Figs. 2(a), 2(b) and 2(b)-relaxed (see column 1 of the same tables) together with the experimental data where available. The model Q'_{20} values have been calculated with respect to the symmetry axis labeled z in all parts of Fig. 2, and the rotational excitations have been estimated by assuming no variation of the corresponding moment of inertia with angular momentum. The good agreements, apparent from Tables I, II, and III, between the experimental data and the predictions of the present model lend support to our approach. Explanation of the way the moments of inertia in Table III have been obtained follows.

All cases of moment of inertia with value $\mathcal{I}<224.9$ fm^2 (see Table III) correspond to rotation of valence nucleons only. That is, in these cases there is not a rigid body rotation of ^{28}Si, i.e., the core (either ^{16}O or ^{12}C) remains a spectator and thus it does not rotate and does not contribute to the

TABLE III. Moment of inertia ($\mathcal{I}$) in fm^2, bandhead energy ($E_{0_n^+}$) in MeV, and rotational band energies ($E_{I_n^+}$) in MeV of ground-state band and four excited rotational bands for ^{28}Si. Numbers in parentheses stand for the corresponding experimental energies in MeV. The model moment of inertia for the 2_1^+ level is 76.6 fm^2, while for the other member states of the ground-state band it is 100.5 fm^2. Predictions shown in quotation marks stand as upper-bound values. Real values could be smaller, corresponding to a moment of inertia $\mathcal{I}>100.5$ fm^2 (see text).

Vertex configuration	$\mathcal{I}$	$E_{0_n^+}$	E_{2^+}	E_{4^+}	E_{6^+}	E_{8^+}	E_{10^+}	E_{12^+}	E_{14^+}	E_{16^+}	E_{18^+}
(Core: 1-16),	76.6/100.5	0.00	1.62	4.13	8.67	14.85	''22.70''	''32.19''	''43.33''	''56.12''	''70.56''
(17-18,29-30),(25-26,37-38),		(0.00)	(1.78[a])	(4.62[a])	(8.54[a])	(15.19[b])					
(27-28,39-40)											
[Core:(1-2,3,-4$_f$),(5,7,11,13),(6,8,12,14)],	207.0	10.27	10.87	12.27	14.48	17.48	21.29	25.90	31.31	37.52	44.53
(17-18,29-30),(19-20,31-32),		(10.27[a])	(10.88[a])	(12.24[a])							
(25-26,37-38),(27-28,39-40)	250.8	10.27	10.77	11.92	13.74	16.22	19.36	23.17	27.63	32.76	38.55
		(10.27[a])	(10.80[a])	(11.93[a])						(32.20	
										$\Gamma=0.72$)[c]	
[Core: (1-2,3-4),(5,7,11,13),(6,8,12,14)],	207.0	24.2	24.8	26.2	28.4	31.4	35.2	39.8	45.2	51.4	58.5
(17-18,29-30),(19-20,31-32),									(46.2,		
(25-26,37-38),(27-28,39-40)									$\Gamma=0.9$)[d]		
	224.9	24.2	24.8	26.0	28.1	30.8	34.3	38.6	43.6	49.3	55.7
									(43.7,		
									$\Gamma=0.6$)[d]		

[a]See Ref. [45].
[b]See Refs. [66–68].
[c]See Refs. [46,47,69].
[d]See Refs. [50,51].

moment of inertia. In the case of $\mathcal{I}\geqslant 224.9$ fm^2, however, besides the valence nucleons, part of the core participates in the rotation. Specifically, in the case of $\mathcal{I}=224.9$ fm^2, the four $1p_{3/2}$ protons participate in the rotation, while in the case of $\mathcal{I}=250.8$ fm^2, both the four $1p_{3/2}$ protons and the four $1p_{3/2}$ neutrons participate in the rotation.

Of special interest is the case of the ground-state band [Fig. 2(a)] for which a different axis of rotation is considered for the 2_1^+ state and a different axis for the members of the band with $I^\pi=4^+$, 6^+, 8^+. This is a result of the fact that the g.s. deformation of ^{28}Si has a triaxial shape and thus rotation of the nucleus is more difficult at low spin values, hence the rotation takes place around the axis of minimum moment of inertia. As the spinning of the nucleus increases at higher values of the angular momentum ($I^\pi=4^+$, 6^+, 8^+), the rotation shifts towards the axis of medium moment of inertia and it is further expected that for some even higher value of the angular momentum ($I^\pi>8^+$) the nucleus will rotate around the axis of maximum moment of inertia. The deviations between the model predictions and the experimental values could, at least partially, be attributed to a mixing of the possible rotations around two or even three axes of rotation of the triaxial ground state shape of ^{28}Si. The values given here are just the main components of this mixing. The number of nucleons participating in the rotation at each of the above three cases could vary. Specifically, for the moment of inertia $\mathcal{I}_{2_1^+}$ all twelve valence nucleons outside the ^{16}O core rotate around the $R_{2_1^+}$ axis, while for the $\mathcal{I}_{I_1^+,I\geqslant 4}$ eight valence nucleons rotate [namely the nucleons whose average positions are numbered (25-26, 37-38) and (27-28, 39-40)] around the $R_{I_1^+,I\geqslant 4}$ axis. Perhaps, at some value of $I^\pi>8^+$ all twelve valence nucleons could rotate around the same axis.

Of great interest are the excited bands of Table III connected with the α-planar configuration of Fig. 2(b)-relaxed (second configuration in the table). The association of these rotational bands with the 0_4^+ state starts from the near coincidence of the excitation of their bandhead (i.e., 10.40 MeV) with the excitation of this level (i.e., 10.27 MeV [45]). With the same main criterion the experimental state candidates have been chosen as member states of these rotational bands, i.e., for both cases of moment of inertia (see column 2 of Table III). For the first case it is assumed that only the valence nucleons of the $1d_{5/2}2s_{1/2}$ shells participate in the rotation, while for the second case it is assumed that, in addition, nucleons of the core, i.e., the nucleons of the $1p_{3/2}$ shell, participate in the rotation, hence the larger value of the moment of inertia (see column 2 of Table III).

Other experimental observations supporting the above choices up to $I^\pi=4^+$ are less clear than desired due to the fact that the experimental information concerning decay schemes is not sufficiently complete. For example, γ-ray transitions between members of the proposed bands are not available and the level decay to unknown levels in the tables of gamma-ray branching ratios for ^{28}Si has a great percentage for many levels [45]. Specifically, the experimental candidate for the 2^+ state at 10.88 MeV has 20% decay rate to other levels which are not specified [45]. The decay of this level to the 2_1^+ level with a rate [45] of 76%, however, lends some support to our proposition that it is a member of

our α-wise rotational band, since the 2_1^+ level is a member of the g.s. band whose α-cluster structure is established. The same support exists for the nature of the 0_4^+ level at 10.27 MeV as bandhead of the rotational band since the decay rate of this level to 2_1^+ is 58% [45]. Finally, the experimental candidacy of the level 4^+ at 12.24 MeV as a member of the proposed rotational band is supported by the fact that this level appears as resonance of the reaction. ^{24}Mg$+\alpha$ [45]. In conclusion, all three listed members of the rotational band with the small value of moment of inertia have some experimental support for their α-cluster structure. Similar support for the listed low members of the other superdeformed band with the large value of moment of inertia is not available and, of course, band members must have common characteristics besides displaying a $I(I+1)$ energy difference. After the present work, perhaps, it is going to be easier for one to detect the necessary cascade of γ-rays between the members of the proposed superdeformed band.

What is very interesting for the verification of the proposed superdeformed band based on the second (larger) moment of inertia of the second configuration in Table III is that the model prediction of 32.76 MeV for $I^\pi=16^+$ is very close to 32.20 MeV measured in Refs. [46,47] for the same spin value. This measurement is based on the excitation function of the 0_2^+-state at 6.049 MeV of ^{16}O and comes as a resonance of the reaction ^{12}C$+^{16}$O. The knowledge that the 0_2^+ state of ^{16}O is a planar state [48,49] supports our predictions that the observed 32.20 MeV state comes from a planar structure [Fig. 2(c)]. Thus, the present work concerning this state supports the relevant speculations already cited in the literature [46,47]. This success may encourage the research for the low lying members of this rotational band.

Also of interest are the last excited rotational bands of Table III (third configuration) which are also connected with the α-planar structure of Fig. 2(c), but correspond to Fig. 2(b) with no relaxation of the numbered 3 and 4 proton average positions. Association of these bands with low experimental candidate levels is not possible at present since the detailed spectrum of ^{28}Si [45] is known only up to about 15 MeV, that is, it is known up to an energy lower than the bandhead of this proposed band at 24.2 MeV. What is very interesting is that the model predictions of 43.6 MeV and 45.2 MeV for $I^\pi=14^+$ at each band are very close to 43.7 MeV and 46.2 MeV measured in Refs. [50,51]. This closeness is even more impressive if one considers the experimental level widths $\Gamma=0.6$ MeV and 0.9 MeV, respectively [50]. These resonances decay preferentially to 0_3^+ (7.20 MeV) state of ^{20}Ne, which from our study of ^{20}Ne [21] corresponds to $8p4h$ structure possessing ^{12}C core as the third configuration here, a fact which is also supported by Ref. [52].

Table IV includes the predictions of the present work from Tables I, II, and III concerning binding energy, rms charge radius, intrinsic quadrupole moment and moment of inertia for the ground state of ^{28}Si together with the experimental data and the results [53,54] of Hartree-Fock (HF), those [55] of unrestricted 16-parameter variation alpha-cluster model (ACM) for the same (as in HF) nucleon-nucleon interaction, and those of Skyrme interaction [56]. This specific ACM approach consulted here leads to the best results and is the one which gives similar results with the HF model [55]. From Table IV it is apparent that all four models

TABLE IV. Binding energy (E_B), rms charge radius ($\langle r^2\rangle_{\rm ch}^{1/2}$), intrinsic electric quadrupole moment (Q'_{20}), symmetry, and average moment of inertia ($\alpha_{\rm av}$) of the ground state for ^{28}Si according to each method listed in column 1.

Method	E_B[a] (MeV)	$\langle r^2\rangle_{\rm ch}^{1/2}$ (fm)	Q'_{20} (fm^2)	Symmetry	$\alpha_{\rm av}$
ACM[b]	154.1	3.27	-68	D_{5h}	
HF[c]	156.2	3.34	-75		
HF[d]	156.2	3.26	-71		
Skyrme[e]					0.230[e]
Present work	245.3	3.21	-69.6		0.214
Expt.	236.5[f]	3.15(5)[g]	-63 ± 18[h]		

[a]For large scale shell model calculations see Ref. [54].
[b]See Ref. [55].
[c]See Ref. [53].
[d]See Ref. [54].
[e]$\alpha_{\rm av}=\Sigma_I\alpha_I(2I+1)/\Sigma_I(2I+1)$; see Ref. [70].
[f]See Ref. [64].
[g]See Ref. [43].
[h]See Refs. [60,65].

(ACM, HF, Skyrme, and isomorphic shell model) give more or less similar results, except those for binding energy, where ACM and HF give substantially different (smaller) values than the present one, which is close to the experimental value.

The ability of the present approach to predict good results simultaneously for many observables, including binding energies (better even than those coming from large scale shell model calculations [56]) (see Tables I–IV), without using adjustable parameters, constitutes a unique character of the model employed. Moreover, the present approach has the advantage of presenting the physical structure of the states. Indeed, in other models, with the exception of the calculations performed with an SU(3)-classified basis [57], the resulting eigenvectors consist of a very large number of small components. Therefore, it is highly impractical to extract information from these models on such structural properties as intrinsic deformation, orbital symmetry, α-clustering, etc., which are quite important for the sd-shell nuclei [58].

Furthermore, it is interesting for one to notice that certain symmetries of Figs. 2(a), 2(b), and 2(b)-relaxed can follow from two simple and well-known properties of all effective shell-model interactions, namely, the exchange nature and the finite range [59]. In addition, the deformed intrinsic states presented by Figs. 2(a), 2(b), and 2(b)-relaxed could be used in any HF treatment of the relevant rotational bands, a fact which obviously relaxes the requirement of rotational invariance for the HF density [59].

An additional interesting feature of the average structures provided by Figs. 2(a), 2(b), and 2(b)-relaxed, particularly apparent from Fig. 2(c), is the hexadecapole deformation of these structures for ^{28}Si (see Q'_{40} values in Table II), a fact which is experimentally verified by scattering of α-particles on this nucleus [60].

IV. CONCLUSIONS

The isomorphic shell model (whose main feature is that the nucleon finite size is taken into account) has been em-

ployed for the study of superdeformed states in ^{28}Si and the results are successfully compared with the experimental data and those of the α-cluster model and of other theories. Oblate triaxial structure for the ground state and an α-particle-wise planar structure for the 0_4^+ state at 10.24 MeV, and possibly for another planar structure at 24.2 MeV, have been found.

Here, α-like particles (which apparently are not preformed) are considered to be clusters of four closeby nucleons (two protons and two neutrons) which are in relative *s*-state. In order to facilitate the comparison of the present results with those of the α-cluster models, the semiclassical part instead of the quantum mechanical part of the isomorphic shell model is here employed.

While for the ground state band only valence nucleons participate in the rotation, in the excited bands part of the ^{12}C core (i.e., the $1p_{3/2}$ nucleons) can participate in the rotation as well.

An interesting result is the prediction that the $2_1{}^+$ rotational level has a different axis of rotation than the $4_1{}^+$, $6_1{}^+$, and $8_1{}^+$ levels and that, perhaps, at some higher angular momentum values, a third axis of rotation is involved in the ground state rotational band. This result emphasizes the difference between rotational bands in light nuclei and those bands in the nuclei of the well deformed region of rare earths where only one axis of rotation characterizes a rotational band. This difference in the rotational bands of these two regions can also be noticed from the fact that the deviations between the present predictions and the experimental data in the ground-state band are larger than the usual deviations in the well deformed region. These larger deviations could be attributed to the fact that adiabaticity between intrinsic motion and rotational motion is not necessarily ensured for light nuclei, to the fact that it is not known to what extent the assumption of fixed intrinsic state is correct [61] for these nuclei, to the fact that there may be mixing of simultaneous rotations around different axes, and to the fact that no variation of the moment of inertia with angular momentum has been considered. The latter cannot be treated in the framework of the variable-moment-of-inertia model [62], since the number of rotational levels known in rotational bands of light nuclei is very limited (usually two to four).

Furthermore, concerning rotational levels one can find it interesting to note that the present way of moment-of-inertia calculation is equivalent to a rotation of α-like nucleon clusters as in Ref. [63].

The 32.20 MeV, $I^\pi = 16^+$ level predicted [46,47] as corresponding to planar structure of ^{28}Si has here been found to be a member of an excited rotational band with almost rigid rotation (see Table III). Since this level is a resonance of the reaction ^{12}C+^{16}O (6.049 MeV), and the 0_2^+ at 6.049 MeV of ^{16}O has been reported as planar state [48,49], the inclusion of this level to the present excited rotational band constitutes a signature of the planar structure for all member states of this band. Also, the ^{16}O+^{12}C resonances in ^{8}Be and α channels [50,51] at 43.7 MeV and 46.2 MeV have here been identified as 14^+ members of two other proposed rotational bands. The knowledge that both of these resonances decay preferentially to 0_3^+ state of ^{20}Ne known for its $8p4h$ structure [62] supports the present study that the related bands have a planar structure.

A very interesting point to be investigated later, when additional experimental information becomes available, is to examine if both bands either of the second and/or of the third configuration in Table III really have low energy members or if the band with larger moment of inertia terminates at some value of angular momentum decaying into the other band of smaller moment of inertia, a phenomenon known from the superdeformed rotational spectra of nuclei in the well-deformed region. If the second case is proved true, the corresponding band will have all the characteristics of a superdeformed rotational band, given that its moment of inertia approaches the rigid body limit (see Table III). Also of interest is the fact that two of the rotational bands in Table III have the same moment of inertia (equal to 207.0 fm^2), something which has also been observed in nuclei of the well-deformed region.

Hexadecapole deformation has been found for both the ground state (relatively small) and the 0_4^+ excited state (relatively large). This finding agrees with the predictions of Ref. [60] that in ^{20}Ne and ^{28}Si such a deformation exists.

The advantage of the present approach is apparent from three facts. First, it predicts better binding energy and other observables, second, uses no adjustable parameters, and third, provides information about the intrinsic structure of the states. This approach is, indeed, superior to the different self-consistent approaches due to the fact that the former is a successful hybrid between the independent particle model and the liquid drop model, while the latter are based on the independent particle model alone.

ACKNOWLEDGMENTS

I want to express my deep appreciation to Dr. P. E. Hodgson of the Nuclear Physics Laboratory (University of Oxford) for his valuable help in all stages of this research. Also, it is my pleasure to thank Dr. A. C. Merchant of the Nuclear Physics Laboratory (University of Oxford) for valuable discussions. Finally, I want to thank the Nuclear Physics Laboratory for its hospitality and also the NCSR ''Demokritos'' for financial support during my sabbatical leave.

[1] W. Wefelmeier, Z. Phys. **107**, 332 (1937).
[2] J. A. Wheeler, Phys. Rev. **32**, 1083 (1937).
[3] D. Dennison, Phys. Rev. **57**, 454 (1940).
[4] J. M. Blatt and V. F. Weisskopf, *Theoretical Nuclear Physics* (Wiley, New York, 1952), p. 292.
[5] D. Dennison, Phys. Rev. **96**, 378 (1954).
[6] S. L. Kameny, Phys. Rev. **103**, 358 (1956).
[7] H. Morinaga, Phys. Rev. **101**, 254 (1956); Phys. Lett. **21**, 78 (1966).

[8] K. Wildermuth and Th. Kanellopoulos, Nucl. Phys. **7**, 150 (1958); **9**, 449 (1958).
[9] D. M. Brink, in *The Alpha-Particle Model of Light Nuclei*, Proceedings of the International School of Physics, ''Enrico Fermi,'' Course XXXVI, edited by C. Bloch (Academic, New York, 1966).
[10] K. Ikeda, N. Takigawa, and H. Horiuchi, Prog. Theor. Phys. Suppl. extra number **40**, 464 (1968).
[11] D. M. Brink, H. Friedrich, A. Weiguny, and C. W. Wong, Phys. Lett. **33B**, 143 (1970).
[12] D. Robson, Phys. Rev. Lett. **42**, 876 (1979).
[13] D. Robson, Phys. Rev. C **25**, 1108 (1982).
[14] W. Bauhoff, H. Schultheis, and R. Schultheis, Phys. Lett. **95B**, 5 (1980); **106B**, 278 (1981); Phys. Rev. C **22**, 861 (1980); **29**, 1046 (1984).
[15] S. Marsh and W. D. M. Rae, Phys. Lett. B **180**, 185 (1986).
[16] P. E. Hodgson, in *Atomic and Nuclear Clusters*, Proceedings of the Second International Conference at Santorini, Greece, 1993, edited by G. S. Anagnostatos and W. von Oertzen (Springer, Berlin, 1995).
[17] A. C. Merchant and W. D. M. Rae, Nucl. Phys. **A549**, 431 (1992).
[18] J. Zhang and W. D. M. Rae, Nucl. Phys. **A564**, 252 (1993).
[19] H. T. Richards, Phys. Rev. C **29**, 276 (1984).
[20] G. S. Anagnostatos, Phys. Rev. C **51**, 152 (1995).
[21] P. K. Kakanis and G. S. Anagnostatos, Phys. Rev. C **54**, 2996 (1996).
[22] P. Tikkanen, J. Keinonen, and A. Kangasmki, Phys. Rev. C **47**, 145 (1993).
[23] G. S. Anagnostatos, Can. J. Phys. **70**, 361 (1992).
[24] W. D. M. Rae, A. C. Merchant, and J. Zhang, Phys. Lett. B **321**, 1 (1994).
[25] G. S. Anagnostatos, Int. J. Theor. Phys. **24**, 579 (1985).
[26] P. E. Hodgson, Contemp. Phys. **35**, 329 (1994).
[27] M. K. Gaidarov, A. N. Antonov, G. S. Anagnostatos, S. E. Massen, M. V. Stoitsov, and P. E. Hodgson, Phys. Rev. C **52**, 3026 (1995).
[28] M. K. Gaidarov, A. E. Antonov, S. E. Massen, and G. S. Anagnostatos, JINR Rapid Communications **80**, 23 (1997).
[29] G. S. Anagnostatos, Int. J. Mod. Phys. E **5**, 557 (1995).
[30] J. Giapitzakis, P. Ginis, A. N. Antonov, S. E. Massen, and G. S. Anagnostatos, Int. J. Mod. Phys. E. (to be published).
[31] W. F. Hornyak, *Nuclear Structure* (Academic, New York, 1975).
[32] J. D. Vergados, *Mathematical Methods in Physics* (Akourastos Giannis, Ioannina, Greece, 1979).
[33] P. Ring and P. Schuck, *The Nuclear Many-Body Problem* (Springer-Verlag, Heidelberg, 1980), p. 189.
[34] E. Merzbacher, *Quantum Mechanics* (Wiley, New York, 1961), p. 42.
[35] C. Cohen-Jannoudji, B. Diu, and F. Laloë, *Quantum Mechanics* (Wiley, New York, 1977), p. 240.
[36] G. S. Anagnostatos, Lett. Nuovo Cimento **22**, 507 (1978); J. Leech, Math. Gaz. **41**, 81 (1957).
[37] G. S. Anagnostatos, Lett. Nuovo Cimento **28**, 573 (1980).
[38] G. S. Anagnostatos, Lett. Nuovo Cimento **29**, 188 (1980).
[39] G. S. Anagnostatos, J. Yapitzakis, and A. Kyritsis, Lett. Nuovo Cimento **32**, 332 (1981).
[40] G. S. Anagnostatos and C. N. Panos, Phys. Rev. C **26**, 260 (1982).
[41] G. S. Anagnostatos and C. N. Panos, Lett. Nuovo Cimento **41**, 409 (1984).
[42] C. N. Panos and G. S. Anagnostatos, J. Phys. G **8**, 1651 (1982).
[43] C. W. de Jager, H. de Vries, and C. de Vries, At. Data Nucl. Data Tables **14**, 479 (1974).
[44] P. H. Stelson and L. Grodzins, Nucl. Data, Sect. A **1**, 21 (1965).
[45] P. M. Endt, Nucl. Phys. **A521**, 1 (1990).
[46] K. Katori, K. Furuno, and T. Ooi, Phys. Rev. Lett. **40**, 1489 (1978).
[47] K. Furuno, K. Katori, T. Aoki, T. Ooi, and J. Sanada, Nucl. Phys. **A321**, 250 (1979).
[48] W. Bauhoff, H. Schultheis, and R. Schultheis, Phys. Rev. C **29**, 1046 (1984).
[49] W. D. M. Rae and A. C. Merchant, Mod. Phys. Lett. A **8**, 2435 (1993).
[50] M. A. Eswaran, S. Kumar, E. T. Mirgule, D. R. Chakrabarty, V. M. Datar, N. L. Ragoowansi, and U. K. Pal, Phys. Rev. C **47**, 1418 (1993).
[51] M. A. Eswaran and S. Kumar, Phys. Rev. C **48**, 2120 (1993).
[52] R. Middleton, J. D. Garrett, and H. T. Fortune, Phys. Rev. Lett. **27**, 950 (1971).
[53] P. U. Sauer, A. Faessler, H. H. Wolter, and M. M. Stingl, Nucl. Phys. **A125**, 257 (1969).
[54] J. Zofka and G. Ripka, Nucl. Phys. **A168**, 65 (1971).
[55] W. Bauhoff, H. Schultheis, and R. Schultheis, Phys. Lett. **106B**, 278 (1981).
[56] B. Cole, A. Watt, and R. R. Whitehead, J. Phys. A **7**, 1374 (1974); J. Phys. G **1**, 213 (1975).
[57] M. Harvey, *Advances in Nuclear Physics, Vol. 1*, edited by M. Baranger and E. Vogt (Plenum, New York, 1968) and quotations herein.
[58] H. Feldmeier and P. Manakos, Z. Phys. A **281**, 379 (1977).
[59] M. K. Banerjee, C. A. Levinson, and G. J. Stephenson, Jr., Phys. Rev. **178**, 1709 (1969).
[60] H. Rebel, G. W. Schweimer, J. Specht, G. Schatz, R. Lhken, D. Habs, G. Hauser, and H. Klewe-Nebenius, Phys. Rev. Lett. **26**, 1190 (1971).
[61] Y. Horikawa, A. Nakada, and Y. Torizuka, Prog. Theor. Phys. **49**, 2005 (1973).
[62] M. A. J. Mariscotti, G. Scharff-Goldhaber, and B. Buck, Phys. Rev. **178**, 1864 (1969).
[63] L. Pauling and A. B. Robinson, Can. J. Phys. **53**, 1953 (1975).
[64] A. H. Wapstra and N. B. Grove, Nucl. Data Tables **9**, 267 (1971).
[65] O. Häusser *et al.*, Phys. Rev. Lett. **23**, 320 (1969).
[66] K. W. Schmid, L. Satpathy, and A. Faessler, Z. Phys. **267**, 345 (1974).
[67] P. M. Endt and C. van der Leun, Nucl. Phys. **A105**, 1 (1967).
[68] J. D. Pearson, E. Almqvist, and J. A. Kuehner, Can. J. Phys. **42**, 489 (1964).
[69] G. J. Gyapong, W. N. Catford, S. Singer, S. Chappell, S. Fox, C. D. Jones, P. Lee, D. L. Watson, M. Freer, R. le Marechal, G. Kelly, and R. P. Ward, Proceedings of the ''Cluster 94'' International Conference at Strasbourg, 1994 (unpublished).
[70] W. Y. Ng and L. E. H. Trainor, Can. J. Phys. **52**, 541 (1974).